AD-A069 884 NORTH CAROLINA STATE UNIV RALEIGH ENGINEERING DESIGN--ETC F/G 21/5
AN ACTUATOR DISK ANALYSIS OF AN ISOLATED ROTOR WITH DISTORTED I--ETC(U)
MAR 79 J N PERKINS F44620-76-C-0055
UNCLASSIFIED NCSU/EDC-79-1 NL

| OF |
AD
AD 6988A

END
DATE
FILMED
7-79
DDC

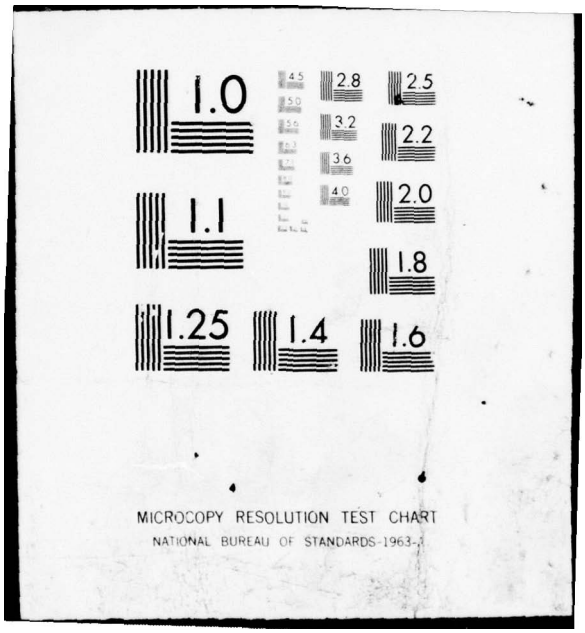
1.0
1.1
1.25
1.4
1.6
1.8
2.0
2.2
2.5
2.8
3.2
3.6
4.0
4.5
5.0
5.6
MICROCOPY RESOLUTION TEST CHART
NATIONAL BUREAU OF STANDARDS-1963-A

ENGINEERING
DESIGN
CENTER

SCHOOL OF
ENGINEERING

NORTH CAROLINA
STATE UNIVERSITY

RALEIGH
NORTH CAROLINA

EDC-79-1

LEVEL II

An Actuator Disk Analysis of an Isolated Rotor with Distorted Inflow

by

J. N. Perkins

Report on AFOSR Contract F44620-76-C-0055
for a cooperative program between
United Technologies Research Center
and
North Carolina State University

An Actuator Disk Analysis of an Isolated Rotor with Distorted Inflow

by

J. N. Perkins

Report on AFOSR Contract F44620-76-C-0055 for a cooperative program

between

United Technologies Research Center
East Hartford, Conn.

and

North Carolina State University
Raleigh, North Carolina

Engineering Design Center
School of Engineering
North Carolina State University
Raleigh, N. C. 27650

March 31, 1979

Abstract

An analytical study of the passage of distorted flow through an isolated, high hub-tip ratio axial compressor is reported. The analysis involves the coupling of the unsteady blade row aerodynamic response (with the flow immediately upstream of the blade row prescribed) with the unsteady duct flow both upstream and downstream of the blade row under the influence of the blade row loading. The numerical solution uses a starting procedure which does not require the inlet plane to be far enough upstream to be unaffected by the presence of the blade row. Hence any experimentally determined distortion at any arbitrary distance upstream of the blade row can be modelled. The results obtained indicate that the predicted pressure profile at the blade row exit is strongly dependent on the experimentally determined steady-state loss and exit flow angle curves, but is almost independent of the magnitude of the first order lag coefficient used to represent the boundary layer time delay through the blade passages.

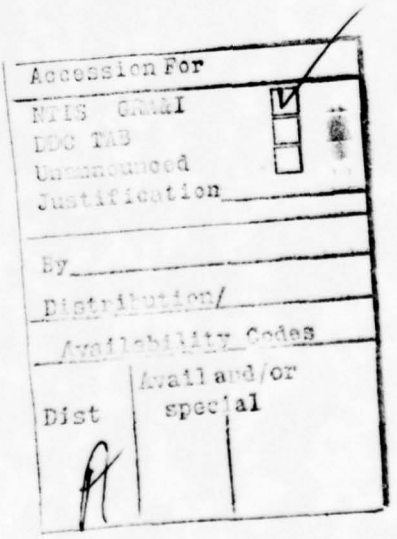

Introduction

The successful prediction of the performance of a bladed compressor requires adequately quantitative mathematical methods for describing the flow behavior encountered in the machine in terms of accurately measurable quantities. In the present study, the response of an isolated rotor to inlet flow distortions is considered.

Of the various inlet flow distortion modes, the uniform radial condition with circumferentially distorted axial flow has been found to have large effects on compressor performance. Thus, this type has been extensively investigated both analytically and experimentally. A useful bibliography can be found in Refs. 1 and 2 which may serve as guides for the current state of the art, and may provide reference lists to the vast literature already existing in the field. Different models have been developed to predict the response of compressors to circumferential inlet distortions and recent examples of the more complete treatments are given in Refs. 3 - 5.

One of the major difficulties inherent in developing such analyses is that the rotor blades, which move through a spatially nonuniform flow field, are subjected to unsteady flow. This unsteady performance is an essential part of any analytical perdiction technique for distorted flow. Although some success has been achieved, the models presently used to describe this unsteady response are still quite rudimentary, and there is considerable room for improvements. One of the major difficulties here is the lack of detailed quantitative knowledge of the unsteady flow field imposed on the blades. In fact, due to this lack of quantitative experimental evidence for isolated rotors, very few, if any, direct comparisons between the existing analytical models and experiment have been made. Therefore, North Carolina State University and United Technologies Research Center have embarked on a joint project under sponsorship of the Air Force Office of Scientific Research to study analytically and experimentally the response of a compressor stage to an inlet distortion. The work reported herein is the first of several planned analytical investigations and direct comparisons to experiment of this phenomen.

Semi-actuator Disk Analysis

A nonlinear, large disturbance theory was developed which couples, interactively, the flow through the passages of an isolated, high hub-tip ratio axial compressor blade row and an axially distorted incompressible flow field. The blade row analysis is based on the time-dependent energy equation developed in Ref. 3. The flow field analysis involves the two-dimensional form of the time-dependent, incompressible, viscous Navier Stokes equations. Coupling of the two is accomplished by satisfying the boundary conditions relating the pressure change across the blade row and those requiring mass continuity through the blade row.

Since the flow is assumed to be independent of radial position, the analysis can be carried out in the two-dimensional cascade plane. This is shown schematically in Fig. 1, which represents the flow field ahead of and behind an axial compressor blade row, unwrapped tangentially and projected onto a two-dimensional plane. The lines ABC and DEF represent a common axial trace in the three-dimensional compressor system, and this correspondence imposes a periododic boundary condition on the flow velocities. A distorted inlet flow is initialized along the inlet boundary AD, and a constant, although unknown a priori, static exit pressure condition is imposed at the exit boundary CF. The blade row represented by the line BE is modelled as a semi-actuator disk across which there is a change in the flow direction as well as a change in total pressure.

The flow field upstream and downstream of the blade row is required to satisfy the incompressible Navier Stokes equations of motion without assuming conservation of mass (see Fig. 1 for nomenclature),

$$\frac{\partial u'}{\partial t'} = -\frac{\partial u'^2}{\partial x'} - \frac{1}{\rho}\frac{\partial p'}{\partial x'} + \nu\left(\frac{\partial^2 u'}{\partial x'^2} + \frac{\partial^2 u'}{\partial y'^2} + \frac{1}{3}\frac{\partial D'}{\partial x'}\right) \tag{1}$$

$$\frac{\partial u'}{\partial t'} = -\frac{\partial v'}{\partial x'} - \frac{\partial u'v'}{\partial x'} - \frac{1}{\rho}\frac{\partial p'}{\partial y'} + \nu\left(\frac{\partial^2 v'}{x'^2} + \frac{\partial^2 v'}{\partial y'^2} + \frac{1}{3}\frac{\partial D'}{\partial y'}\right) \tag{2}$$

and the equation of continuity,

$$D' = \frac{\partial u'}{\partial y'} + \frac{\partial v'}{\partial y'} \tag{3}$$

The mass discrepancy term, D', should ideally be zero. However, due to inaccuracies in the finite difference computations, this term, while required to be small, is not zero and is left in the equations to eliminate a nonlinear instability in the solution.

Introducing the nondimensional quantities:

$$u = u'/U \quad , \quad v = v'/U \quad , \quad p = p'/\rho U^2$$

$$x = x'/\ell \quad , \quad y = y'/\ell \quad , \quad t = t'U/\ell \tag{4}$$

eqs. (1) - (3) become

$$\frac{\partial u}{\partial t} = -\frac{\partial u^2}{\partial x} - \frac{\partial uv}{\partial y} - \frac{\partial p}{\partial x} + \frac{1}{Re}\left(\frac{\partial^2 u}{\partial x^2} + \frac{\partial^2 u}{\partial y^2} + \frac{1}{3}\frac{\partial D}{\partial x}\right) \tag{5}$$

$$\frac{\partial v}{\partial t} = -\frac{\partial v^2}{\partial y} - \frac{\partial uv}{\partial x} - \frac{\partial p}{\partial y} + \frac{1}{Re}\left(\frac{\partial^2 v}{\partial x^2} + \frac{\partial^2 v}{\partial y^2} + \frac{1}{3}\frac{\partial D}{\partial y}\right) \tag{6}$$

$$D = \frac{\partial u}{\partial x} + \frac{\partial v}{\partial y} \tag{7}$$

By differentiating (5) with respect to x, (6) with respect to y, and (7) with respect to t, Poisson's equation for the pressure can be obtained as follows:

$$\frac{\partial^2 u}{\partial x \partial t} = -\frac{\partial^2 u^2}{\partial x^2} - \frac{\partial^2 uv}{\partial x \partial y} - \frac{\partial^2 p}{\partial x^2} + \frac{1}{Re}\left(\frac{\partial^3 u}{\partial x^3} + \frac{\partial^3 u}{\partial x \partial y^2} + \frac{1}{3}\frac{\partial^2 D}{\partial x^2}\right)$$

$$\frac{\partial^2 v}{\partial y \partial t} = -\frac{\partial^2 v^2}{\partial y^2} - \frac{\partial^2 uv}{\partial x \partial y} - \frac{\partial^2 p}{\partial y^2} + \frac{1}{Re}\left(\frac{\partial^3 v}{\partial x \partial y} + \frac{\partial^3 v}{\partial y^3} + \frac{1}{3}\frac{\partial^2 D}{\partial y^2}\right)$$

$$\frac{\partial D}{\partial t} = \frac{\partial^2 u}{\partial x \partial t} + \frac{\partial^2 v}{\partial y \partial t}$$

$$\frac{\partial D}{\partial t} = -\frac{\partial^2 u^2}{\partial x^2} - \frac{\partial^2 v^2}{\partial y^2} - 2\frac{\partial^2 uv}{\partial x \partial y} - \frac{\partial^2 p}{\partial x^2} - \frac{\partial^2 p}{\partial y^2} + \frac{1}{Re}\left[\frac{\partial^3 u}{\partial x^3} + \frac{\partial^3 v}{\partial x^2 \partial y} + \frac{\partial^3 u}{\partial y^2 \partial x}\right.$$

$$\left. + \frac{\partial^3 v}{\partial y^3} + \frac{1}{3}\left(\frac{\partial^2 D}{\partial x^2} + \frac{\partial^2 D}{\partial y^2}\right)\right]$$

$$\frac{\partial^2 p}{\partial x^2} + \frac{\partial^2 p}{\partial y^2} = -\frac{\partial^2 u^2}{\partial x^2} - \frac{\partial^2 v^2}{\partial y^2} - 2\frac{\partial^2 uv}{\partial x \partial y} - \frac{\partial D}{\partial t} + \frac{1}{Re}\left[\frac{\partial^2}{\partial x^2}\left(\frac{\partial u}{\partial x} + \frac{\partial v}{\partial y}\right) + \frac{\partial^2}{\partial y^2}\left(\frac{\partial u}{\partial x} + \frac{\partial v}{\partial y}\right)\right.$$

$$\left. + \frac{1}{3}\left(\frac{\partial^2 D}{\partial x^2} + \frac{\partial^2 D}{\partial y^2}\right)\right]$$

$$\frac{\partial^2 p}{\partial x^2} + \frac{\partial^2 p}{\partial y^2} = -R \tag{8}$$

$$R \equiv \frac{\partial^2 u^2}{\partial x^2} + \frac{\partial^2 v^2}{\partial y^2} + 2\frac{\partial^2 uv}{\partial x \partial y} + \frac{\partial D}{\partial t} - \frac{4}{3}\frac{1}{Re}\left[\frac{\partial^2 D}{\partial x^2} + \frac{\partial^2 D}{\partial y^2}\right] \tag{9}$$

Note that for the flow under consideration, the value of D should be very small before the above equations can be said to model the flow accurately. The mass discrepancy term is retained for the sole purpose of eliminating a nonlinear instability in the computer solution.

By assuming that the flow in the blade passage of the cascade is like channel flow, the unsteady blade row equations can be derived as in Reference 3:

$$\frac{1}{\rho}(P'_{0_1} - P'_{0_2}) = c \sec \xi\left(\frac{u'}{t'}\right)_r + \frac{1}{2}X[u'_1 + (V'+v')_1] \tag{10}$$

where X is an unsteady loss parameter defined as the instantaneous sum of the gap-averaged deviation of exit total pressure and the dissipated mechanical energy during an unsteady process. In a steady-state process eq. (10) shows that X reduces to the standard steady-state loss coefficient,

$$X_{ss} = \frac{P'_{0_1} - P'_{0_1}}{1/2\rho[u'^2+(V'+v'_1)^2]} \tag{11}$$

Since the specific unsteady behavior of X is not known, the first-order lag model of ref. (3) is used:

$$X = X_{ss} - \tau'\left(\frac{\partial X}{\partial t'}\right)_r \tag{12}$$

Figure 2 shows the stationary and blade reference frames. The time derivatives in the blade reference frame are transferred to the stationary frame by:

$$\left(\frac{\partial}{\partial t'}\right)_r = \left(\frac{\partial}{\partial t'}\right) - V'\left(\frac{\partial}{\partial y'}\right) \tag{13}$$

and the blade row equations become:

$$\frac{1}{\rho}(P'_{0_1} - P'_{0_2}) = c \sec \xi\left(\frac{\partial u_1'}{\partial t'} - V'\frac{\partial u_1'}{\partial y'}\right) + \frac{1}{2}X[u_1'^2 + (V' + v_1')^2] \tag{14}$$

and

$$X = X_{ss} - \tau'\left(\frac{\partial X}{\partial t'} - V'\frac{\partial X}{\partial y'}\right) \tag{15}$$

Since continuity across the blade channel requires

$$u'_1 = u'_2 \equiv u' \quad , \tag{16}$$

then from Fig. 2 it can be seen that

$$\cot \beta_1 = \frac{V'+v_1'}{u'} \quad , \quad \cot \beta_2 = \frac{V'+v_2'}{u'} \tag{17}$$

Using Bernoulli's equation at the inlet and exit plane,

$$\begin{aligned} P'_{0_1} &= p_1' + \frac{1}{2}\rho[u'^2 + (V'+v')^2] \\ P'_{0_2} &= p_2' + \frac{1}{2}\rho[u'^2 + (V'+v')^2] \end{aligned} \tag{18}$$

Using eqs. (17) and (18), eq. (14) can be written:

$$\frac{1}{\rho}(p_1'-p_2') = c' \sec \xi \left[\frac{\partial u'}{\partial t'} - V'\frac{\partial u'}{\partial y'}\right] + \frac{1}{2}u'^2[X+(X-1)\cot^2\beta_1 + \cot^2\beta_2] \tag{19}$$

Introducing the additional dimensionless quantities

$$V = V'/U, \qquad c = c'/\ell \ , \qquad \tau = \tau' U/\ell \tag{20}$$

and using eqs. (4), the dimensionless blade row coupling equations become:

$$P_1 - P_2 = c \sec \xi \left[\frac{\partial u}{\partial t} - V\frac{\partial u}{\partial y}\right] + \frac{1}{2}u^2[X + (X-1)\cot^2\beta_1 + \cot^2\beta_2] \tag{21}$$

where

$$X = X_{ss} - \tau\left(\frac{\partial X}{\partial t} - V\frac{\partial X}{\partial y}\right) \tag{22}$$

The values of X_{ss} and β_2 as functions of β_1 and the value of τ must be determined from experiment. Equations (5) through (9), (21) and (22) are the partial differential equations to be solved. However, before a solution can be attempted, it is necessary to have suitable boundary and initial conditions.

Figure 1 illustrates the six boundaries of importance in this problem. The upper and lower boundaries are the easiest to handle. All conditions on the lower boundary are equal to those on the upper boundary. This is equivalent to saying in the case of the actual rotor that conditions are periodic around the circumference.

It will be assumed that the inlet is far enough away from the blade row so that:

$$\frac{\partial v}{\partial x} = 0 \qquad \frac{\partial D}{\partial x} = 0 \tag{23}$$

By applying continuity, another condition can be found:

$$\frac{\partial u}{\partial x} = D - \frac{\partial v}{\partial y} \tag{24}$$

Differentiating (10) with respect to x yields:

$$\frac{\partial^2 u}{\partial x^2} = \frac{\partial D}{\partial x} - \frac{\partial}{\partial y}\left(\frac{\partial v}{\partial x}\right) = 0 \tag{25}$$

It will also be assumed that the total pressure remains constant with time along the inlet. Differentiating Bernoulli's equation with respect to t gives:

$$\frac{\partial p}{\partial t} = -\frac{1}{2}\left(\frac{\partial u^2}{\partial t} + \frac{\partial v^2}{\partial t}\right) \tag{26}$$

For the outlet, assumptions (23), (24), and (25) are used again. These conditions are applied in (5) to formulate the Neumann pressure gradient boundary condition:

$$\frac{\partial p}{\partial x} = -\frac{\partial u^2}{\partial x} - \frac{\partial uv}{\partial y} + \frac{1}{Re}\frac{\partial^2 u}{\partial y^2} \tag{27}$$

Note that in the above $\frac{\partial u}{\partial t}$ has been neglected.

The most complicated boundary conditions occur at the blade row entrance and exit. Assumptions (23), (24), and (25) will be utilized at both entrance and exit along with:

$$D = 0 \quad , \quad \frac{\partial u}{\partial x} = -\frac{\partial v}{\partial y} \tag{28}$$

The pressure gradient at entrance and exit can be found as before:

$$\left(\frac{\partial p}{\partial x}\right)_1 = -\left(\frac{\partial u}{\partial t}\right)_1 - \left(\frac{\partial u^2}{\partial x}\right)_1 - \left(\frac{\partial uv}{\partial y}\right)_1 + \frac{1}{Re}\left(\frac{\partial^2 u}{\partial y^2}\right)_1 \tag{29}$$

$$\left(\frac{\partial p}{\partial x}\right)_2 = -\left(\frac{\partial u}{\partial t}\right)_2 - \left(\frac{\partial u^2}{\partial x}\right)_2 - \left(\frac{\partial uv}{\partial y}\right)_2 + \frac{1}{Re}\left(\frac{\partial^2 u}{\partial y^2}\right)_2 \tag{30}$$

The unsteady term must be included here. From continuity across the blade channel:

$$\left(\frac{\partial u}{\partial t}\right)_1 = \left(\frac{\partial u}{\partial t}\right)_2 \quad , \quad \left(\frac{\partial^2 u}{\partial y^2}\right)_2 = \left(\frac{\partial^2 u}{\partial y^2}\right)_2 \tag{31}$$

Subtracting (30) from (29) and applying (31) leads to an expression coupling the pressure fields on either side of the blade row:

$$\left(\frac{\partial p}{\partial x}\right)_1 - \left(\frac{\partial p}{\partial x}\right)_2 = \left(\frac{\partial u^2}{\partial x}\right)_2 - \left(\frac{\partial u^2}{\partial x}\right)_1 + \left(\frac{\partial uv}{\partial y}\right)_2 - \left(\frac{\partial uv}{\partial y}\right)_1 \tag{32}$$

Initial conditions compatible with the above boundary conditions are needed to start the problem. The initial inlet axial velocity and pressure distributions are obtained from curve fits of experimental data. The initial inlet axial velocity distribution will be assumed constant in x up to and including the blade row exit. The circumferential velocity will be zero in the entire upstream region. From this information values of β_1 and corresponding values of β_2 can be generated. This will give the circumferential velocity distribution behind the blade row. From continuity:

$$\left(\frac{\partial u}{\partial x}\right)_2 = \left(\frac{\partial v}{\partial y}\right)_2 \tag{33}$$

As a starting point, it is assumed that behind the blade row:

$$\frac{\partial u}{\partial x} = \left(\frac{\partial u}{\partial x}\right)_2 e^{-A(x-x_2)} \tag{34}$$

Again applying continuity:

$$\frac{\partial v}{\partial y} = -\left(\frac{\partial u}{\partial x}\right)_2 e^{-A(x-x_2)} \tag{35}$$

Also along the center line behind the blade row, it is arbitrarily assumed that initially

$$\frac{\partial v}{\partial x} = 0 \tag{36}$$

Note that D equals zero everywhere initially.

Also:

$$\frac{\partial X}{\partial t} = 0 \tag{37}$$

The next step in the analysis consists of finite differencing the above partial differential expressions. The differencing technique used is that of Welch, et. al. (Ref. 6). The results along with the mesh setup are given in the appendix.

The numerical procedure used to obtain the solution to the finite differenced equations and associated boundary conditions as given in the appendix employs the algorithm for solving elliptic problems by direct marching methods given by Roach in Ref. (7). This method was used because it was found to be at least two orders of magnitude faster than any other method which did not diverge. While the marching algorithm is field size limited, no problems were noted with the present field size which extended from approximately 4 chord lengths upstream of the blade row to approximately 15 chord lengths downstream of the blade row. The starting procedure is to initialize an axial velocity distortion at t = 0 at the inlet plane, AD, and, assuming no work being done on the fluid at this plane, maintain the resulting total pressure at the inlet constant for all later times. This does not require making the usual assumption that the inlet plane is far enough upstream to be unaffected by the presence of the blade row at BE. At each time step over t > 0, the propagation through the entire flow field of the disturbances created by the blade row is computed subject to a simultaneous satisfaction of all boundary conditions. The computation is terminated when a steady state solution is obtained. The resulting axial distortion is then compared to the experimentally determined distortion at the upstream location where the measurements were made. If the two distortions are not identical, the initial distortion at the inlet plane is changed and the computation repeated.

Numerical Results

The finite difference equations and associated boundary conditions given in the appendix were programmed for the NCSU IBM 370 digital computer and a number of cases corresponding to the experimental results presented in Ref. 8 were examined. The required values of X_{ss} and β_2 as functions of β_1 which were used in the computations are presented in Figs. 3 and 4 respectively, and were obtained from the experimental results of Ref. 8. As was noted in Ref. 8, both the loss and turning characteristics as obtained in that study

were thought to be in error. Thus, the results obtained from the present theoretical model are also thought to be in error. In addition, measurements made with a hot wire probe behind the blade row indicated that substantial spanwise flow over the blades existed in the low velocity region of the distortion causing the flow over the blades to be three dimensional. Since the analysis holds only for two-dimensional flow, only qualitative comparisons between the theoretical and experimental results can be made although in each case studied the analytical upstream axial velocities were essentially matched to those obtained experimentally.

Results for the typical case corresponding to an average $\bar{\beta}_1 = 42.2°$ are shown in Figs. 5 - 9. Figure 5 shows the axial velocity of distortion measured approximately 1.2 chord lengths in front of the blade row leading edge and the corresponding distortion predicted analytically. It is believed that the agreement is within the accuracy of the experimental results.

A comparison of the static pressure rise across the blade row as determined experimentally and analytically is presented in Fig. 6. It is seen that the analytical curve exhibits the same general behavior as the experimental data. The differences in the magnitudes of the two results are thought to be due to errors in the experimentally determined loss curve and exit flow angle curve used in the theoretical model and the fact that the flow through the blade row was not two dimensional. It should be noted that changing the magnitude of τ, the time constant of the boundary layer time delay, in eq. (22) causes the analytical pressure rise curve to shift in the circumferential direction without any appreciable change in its shape.

Figures 7 - 9 are "carpet plots" of the static pressure, resultant velocity, and total pressure throughout the entire analytically defined flow field. The slight "ripple" in the axial direction of the total velocity and hence total pressure is apparently due to numerical instabilities in the numerical solution. It should be noted that since the plot routine reduced the axial distance by a factor of two, these instabilities are not as severe as they appear in the figures.

References

1. Mokelke, H: Prediction Techniques. Article in Distortion Induced Engine Instability, AGARD Lecture Series No. 72, (1974).

2. Williams, D.D. and R.G. Hercock: Aerodynamic Response. Article in Distortion Induced Engine Instability, AGARD Lecture Series No. 72, (1974).

3. Adamczyk, J. J.: Unsteady Fluid Dynamic Response of an Isolated Rotor with Distorted Inflow. AIAA paper 74-49, (1974).

4. Mazzawy, R.S." Multiple Segment Parallel Compressor Model for Circumferential Flow Distortion. ASME Journal of Engineering for Power. April 1977, pp. 288-296.

5. Hawthorne, W.R., N.A. Mitchell, J.E. McCune, and C.S. Tan: Nonaxisymmetric Flow Through Annular Actuator Disks: Inlet Distortion Problem. ASME Paper 78-GT-80, (1978).

6. Welch, J.E., F.H. Harlow, J.P. Shannon, and B.J. Daly: The MAC Method. Los Alamos Scientific Laboratory Report No. LA-3425, (1966).

7. Roach, P.J.: Computational Fluid Dynamics. Hermosa Publishers. Albuquerque, New Mexico, (1976).

8. Hardin, L.W. and F.O. Carta: The Response of an Isolated Rotor to a Low Frequency Inlet Distortion. EDC Report 78-1, Engineering Design Center, North Carolina State University, (1978).

Appendix

The coordinate system used in the calculations covers the entire domain of interest with a rectangular grid of cells, each of dimensions Δx by Δy. The cells are numbered by indices i and j, with i counting the columns in the x-direction and j counting the rows in the y-direction. The field-variable values describing the flow field are directly associated with these cells. Their points of definition, relative to a cell, are shown in the figure below:

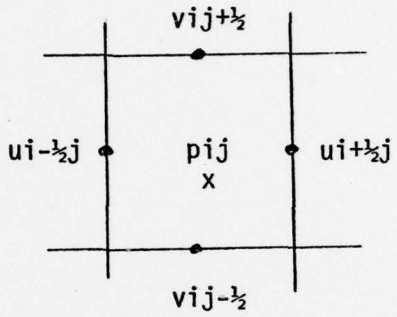

Field-variable layout

As pointed out if Ref. 6, the placement of the field-variable quantities relative to the mesh is of considerable importance to the matter of conservation. In fact, no other arrangement other than the one shown in the figure appears to be workable.

The conservation equations, blade row coupling equations and associated boundary conditions in finite form are as follows:

I. The Continuity Equation:

$$D_{ij} = \frac{1}{\Delta x}(u_{i+\frac{1}{2}j} - u_{i-\frac{1}{2}j}) + \frac{1}{\Delta y}(v_{ij+\frac{1}{2}} - v_{ij-\frac{1}{2}}) \qquad (A.1)$$

II. The Momentum Equations:

$$u_{i+\frac{1}{2}j}^{n+1} = \frac{K\Delta t}{3\Delta x}(D_{i+1j} - D_{ij}) + \frac{\Delta t}{4\Delta y}[(u_{i+\frac{1}{2}j-1} + u_{i+\frac{1}{2}j})\,(v_{i+1j-\frac{1}{2}}$$

$$+ v_{ij-\frac{1}{2}}) - (u_{i+\frac{1}{2}j+1} + u_{i+\frac{1}{2}j})\,(v_{i+1j+\frac{1}{2}} + v_{ij+\frac{1}{2}})]$$

$$+ \frac{\Delta t}{4\Delta x}[(u_{i+\frac{1}{2}j} + u_{i-\frac{1}{2}j})^2 - (u_{i+\frac{3}{2}j} + u_{i+\frac{1}{2}j})^2] + \frac{\Delta t}{\Delta x}(p_{ij}$$

$$- p_{i+1j}) + \frac{K\Delta t}{\Delta x^2}(u_{i+\frac{3}{2}j} + u_{i-\frac{1}{2}j}) + \frac{K\Delta t}{\Delta y^2}(u_{i+\frac{1}{2}j+1}$$

$$+ u_{i+\frac{1}{2}j-1}) + [1-2(\frac{K\Delta t}{\Delta x^2} + \frac{K\Delta t}{\Delta y^2})]\,u_{i+\frac{1}{2}j} \qquad (A.2)$$

$$v_{ij+\frac{1}{2}}^{n+1} = \frac{K\Delta t}{3\Delta y}(D_{ij+1} - D_{ij}) + \frac{\Delta t}{4\Delta y}[(v_{ij-\frac{1}{2}} + v_{ij+\frac{1}{2}})^2 - (v_{ij+\frac{3}{2}} + v_{ij+\frac{1}{2}})^2]$$

$$+ \frac{\Delta t}{4\Delta x}[(u_{i-\frac{1}{2}j+1} + u_{i-\frac{1}{2}j})\,(v_{i-1j+\frac{1}{2}} + v_{ij+\frac{1}{2}}) - (u_{i+\frac{1}{2}j+1}$$

$$+ u_{i+\frac{1}{2}j})\,(v_{i+1j+\frac{1}{2}} + v_{ij+\frac{1}{2}})] + \frac{\Delta t}{\Delta y}(p_{ij} - p_{ij+1})$$

$$+ \frac{K\Delta t}{\Delta x^2}(v_{i+1j+\frac{1}{2}} + v_{i-1j+\frac{1}{2}}) + \frac{K\Delta t}{\Delta y^2}(v_{ij+\frac{3}{2}} + v_{ij-\frac{1}{2}})$$

$$+ [1-2(\frac{K\Delta t}{\Delta x^2} + \frac{K\Delta t}{\Delta y^2})]u_{i+\frac{1}{2}j} \qquad (A.3)$$

III. The Pressure Equations

$$p_{ij} = [\frac{\Delta x^2\Delta y^2}{2(\Delta x^2+\Delta y^2)}]R_{ij} + [\frac{\Delta y^2}{2(\Delta x^2+\Delta y^2)}]\,(p_{i+1j} + p_{i-1j})$$

$$+[\frac{\Delta x^2}{2(\Delta x^2+\Delta y^2)}]\,(p_{ij+1} + p_{ij-1}) \qquad (A.4)$$

where,

$$R_{ij} = -\frac{4K}{3\Delta x^2}(D_{i+1j} + D_{i-1j}) - \frac{4K}{3\Delta y^2}(D_{ij+1} + D_{ij-1}$$

$$+ [\frac{8}{3}(\frac{K}{\Delta x^2} + \frac{K}{\Delta y^2}) - \frac{1}{\Delta t}]D_{ij} + \frac{1}{4\Delta y^2}[(v_{ij+\frac{3}{2}} + v_{ij+\frac{1}{2}})^2$$

$$+ (v_{ij-\frac{3}{2}} + v_{ij-\frac{1}{2}})^2 - 2(v_{ij+\frac{1}{2}} + v_{ij-\frac{1}{2}})^2]$$

$$+ \frac{1}{2\Delta x\Delta y}[(u_{i+\frac{1}{2}j+1} + u_{i+\frac{1}{2}j})(v_{i+1j+\frac{1}{2}} + v_{ij+\frac{1}{2}})$$

$$+ (u_{i-\frac{1}{2}j-1} + u_{i-\frac{1}{2}j})(v_{i-1j-\frac{1}{2}} + v_{ij-\frac{1}{2}}) - (u_{i+\frac{1}{2}j-1}$$

$$+ u_{i+\frac{1}{2}j})(v_{i+1j-\frac{1}{2}} + v_{ij-\frac{1}{2}}) - (u_{i-\frac{1}{2}j+1}$$

$$+ u_{i-\frac{1}{2}j})(v_{i-1j+\frac{1}{2}} + v_{ij+\frac{1}{2}})] + \frac{1}{4\Delta x^2}[(u_{i+\frac{3}{2}j}$$

$$+ u_{i+\frac{1}{2}j})^2 + (u_{i-\frac{3}{2}j} + u_{i-\frac{1}{2}j})^2 - 2(u_{i+\frac{1}{2}j} + u_{i-\frac{1}{2}j})^2] \qquad (A.5)$$

IV. The Blade Row Coupling Equations:

$$p_{ij} = p_{i+3j} + \frac{c \sec \xi}{2\Delta t}(u^{n+1}_{i+\frac{1}{2}j} + u^{n+1}_{i-\frac{1}{2}j} - u_{i+\frac{1}{2}j} - u_{i-\frac{1}{2}j})$$

$$- \frac{V\, c \sec \xi}{4\Delta y}(u_{i+\frac{1}{2}j+1} + u_{i+\frac{1}{2}j} + u_{i-\frac{1}{2}j} + u_{i-\frac{1}{2}j+1}$$

$$- u_{i+\frac{1}{2}j-1} - u_{i+\frac{1}{2}j} - u_{i-\frac{1}{2}j-1} - u_{i-\frac{1}{2}j}) + \frac{1}{8}(u_{i+\frac{1}{2}j}$$

$$+ u_{i-\frac{1}{2}j})^2[X_j + (X_j - 1)\cot^2 \beta_{1j} + \cot^2 \beta_{2j}] \qquad (A.6)$$

where,

$$p_{i+3j} = \frac{c \sec \xi}{2\Delta t}(u_{i+\frac{1}{2}j} + u_{i-\frac{1}{2}j} - u^{n+1}_{i+\frac{1}{2}j} - u^{n+1}_{i-\frac{1}{2}j}) + p_{ij}$$

$$+ \frac{V\, c \sec \xi}{4\Delta y}(u_{i+\frac{1}{2}j+1} + u_{i-\frac{1}{2}j+1} - u_{i+\frac{1}{2}j-1} - u_{i-\frac{1}{2}j-1}$$

$$- \frac{1}{8}(u_{i+\frac{1}{2}j} + u_{i-\frac{1}{2}j})^2[X_j + (X_j - 1)\cot^2 \beta_{1j} + \cot^2 \beta_{2j}] \qquad (A.7)$$

$$\beta_{ij} = \tan^{-1}[(u_{i+\frac{1}{2}j} + u_{i-\frac{1}{2}j}) / (2V + v_{ij+\frac{1}{2}} + v_{ij-\frac{1}{2}})] \quad (A.8)$$

$$\beta_{2j} = \tan^{-1}[(u_{i+\frac{7}{2}j} + u_{i+\frac{5}{2}j}) / (2V + v_{i+3j+\frac{1}{2}} + v_{ij-\frac{1}{2}})] \quad (A.9)$$

$$X_j^{n+1} = \frac{\Delta t}{\tau} X_{ss_j} + (1 - \frac{\Delta t}{\tau}) X_j + \frac{\tau V}{2\Delta y}(X_{j+1} - X_{j-1}) \quad (A.10)$$

Note if $X_j^{n+1} = X_j$:

$$Xj = X_{ss_j} + \frac{\tau V}{2\Delta y}(X_{j+1} - X_{j-1}) \quad (A.11)$$

And if $X_{j+1} = X_j$:

$$X_j = X_{ss\ j} \quad (A.12)$$

V. Inlet Boundary Conditions

$$v_{i-1j-\frac{1}{2}} = V_{i,j-\frac{1}{2}}\ , \qquad v_{i-1j+\frac{1}{2}} = v_{ij+\frac{1}{2}} \quad (A.13)$$

$$D_{i-1j} = D_{ij} \quad (A.14)$$

$$p_{ij}^{n+1} = \frac{1}{8}[(v_{ij+\frac{1}{2}} + v_{ij-\frac{1}{2}})^2 - (v_{ij+\frac{1}{2}}^{n+1} + v_{ij-\frac{1}{2}}^{n+1})^2 + (u_{i+\frac{1}{2}j} + u_{i-\frac{1}{2}j})^2 - (u_{i+\frac{1}{2}j}^{n+1} + u_{i-\frac{1}{2}j}^{n+1})^2] + p_{ij} \quad (A.15)$$

$$u_{i-\frac{3}{2}j} = - u_{i+\frac{1}{2}j} + 2u_{i-\frac{1}{2}j} \quad (A.16)$$

VI. Outlet Boundary Conditions

$$V_{i+1j+\frac{1}{2}} = v_{ij+\frac{1}{2}} \qquad v_{i+1j-\frac{1}{2}} = v_{ij-\frac{1}{2}} \quad (A.17)$$

$$D_{i+1j} = D_{ij} \quad (A.18)$$

$$u_{i+\frac{3}{2}j} = -u_{i-\frac{1}{2}j} + 2u_{i+\frac{1}{2}j} \quad (A.19)$$

$$p_{i+1j} = \frac{K\Delta x}{\Delta y^2}(u_{i+\frac{1}{2}j+1} + u_{i+\frac{1}{2}j-1} - 2u_{i+\frac{1}{2}j})$$

$$+ \frac{\Delta x}{4\Delta y}[(u_{i+\frac{1}{2}j-1} + u_{i+\frac{1}{2}j})\ (v_{i+1j-\frac{1}{2}} + v_{ij-\frac{1}{2}})$$

$$- (u_{i+\frac{1}{2}j+1} + u_{i+\frac{1}{2}j})\ (v_{i+1j+\frac{1}{2}} + v_{ij+\frac{1}{2}})]$$

$$+ \frac{1}{4}[(u_{i+\frac{1}{2}j} + u_{i-\frac{1}{2}j}) - (u_{i+\frac{3}{2}j} + u_{i+\frac{1}{2}j})^2]$$

$$+ p_{ij} \qquad \text{(A.20)}$$

VII. Blade Row Entrance Boundary Conditions:

$$v_{i+1j-\frac{1}{2}} = v_{ij-\frac{1}{2}} \quad , \quad v_{i+1j+\frac{1}{2}} = v_{ij+\frac{1}{2}} \qquad \text{(A.21)}$$

$$D_{i+1j} = D_{ij} = 0 \qquad \text{(A.22)}$$

$$u_{i+\frac{3}{2}j} = - u_{i-\frac{1}{2}j} + 2u_{i+\frac{1}{2}j} \qquad \text{(A.23)}$$

$$p_{i+1j} = \frac{K\Delta x}{\Delta y^2}(u_{i+\frac{1}{2}j+1} + u_{i+\frac{1}{2}j-1} - 2u_{i+\frac{1}{2}j}) + \frac{\Delta x}{4\Delta y}[(u_{i+\frac{1}{2}j-1}$$

$$+ u_{i+\frac{1}{2}j})\ (v_{i+1j-\frac{1}{2}} + v_{ij-\frac{1}{2}}) - (u_{i+\frac{1}{2}j+1}$$

$$+ u_{i+\frac{1}{2}j})\ (v_{i+1j+\frac{1}{2}} + v_{ij+\frac{1}{2}})] = \frac{\Delta x}{\Delta t}(u_{i+\frac{1}{2}j} - u^{n+1}_{i+\frac{1}{2}j})$$

$$+ \frac{1}{4}[(u_{i+\frac{1}{2}j} + u_{i-\frac{1}{2}j})^2 - (u_{i+\frac{3}{2}j} + u_{i+\frac{1}{2}j})^2] + p_{ij} \qquad \text{(A.24)}$$

VIII. Blade Row Exit Boundary Conditions:

$$v_{i-1j-\frac{1}{2}} = v_{ij-\frac{1}{2}} \qquad v_{i-1j+\frac{1}{2}} = v_{ij+\frac{1}{2}} \qquad \text{(A.25)}$$

$$D_{i-1j} = D_{ij} = 0 \qquad \text{(A.26)}$$

$$u_{i-\frac{3}{2}j} = - u_{i+\frac{1}{2}j} = 2u_{i-\frac{1}{2}j} \qquad \text{(A.27)}$$

$$p_{i-1j} = \frac{K\Delta x}{\Delta y^2}(-u_{i-\frac{1}{2}j+1} - u_{i-\frac{1}{2}j-1} + 2u_{i-\frac{1}{2}j})$$

$$+ \frac{\Delta x}{4\Delta y}[(u_{i-\frac{1}{2}j+1} + u_{i-\frac{1}{2}j})\,(v_{ij+\frac{1}{2}} + v_{i-1j+\frac{1}{2}})$$

$$- (u_{i-\frac{1}{2}j-1} + u_{i-\frac{1}{2}j})\,(v_{ij-\frac{1}{2}} + v_{i-1j-\frac{1}{2}})]$$

$$+ \frac{\Delta x}{\Delta t}(u^{n+1}_{i-\frac{1}{2}j} - u_{i-\frac{1}{2}j}) + \frac{1}{4}[(u_{i+\frac{1}{2}j} + u_{i-\frac{1}{2}j})^2$$

$$- (u_{i-\frac{3}{2}j} + u_{i-\frac{1}{2}j})^2] + p_{ij} \qquad \text{(A.28)}$$

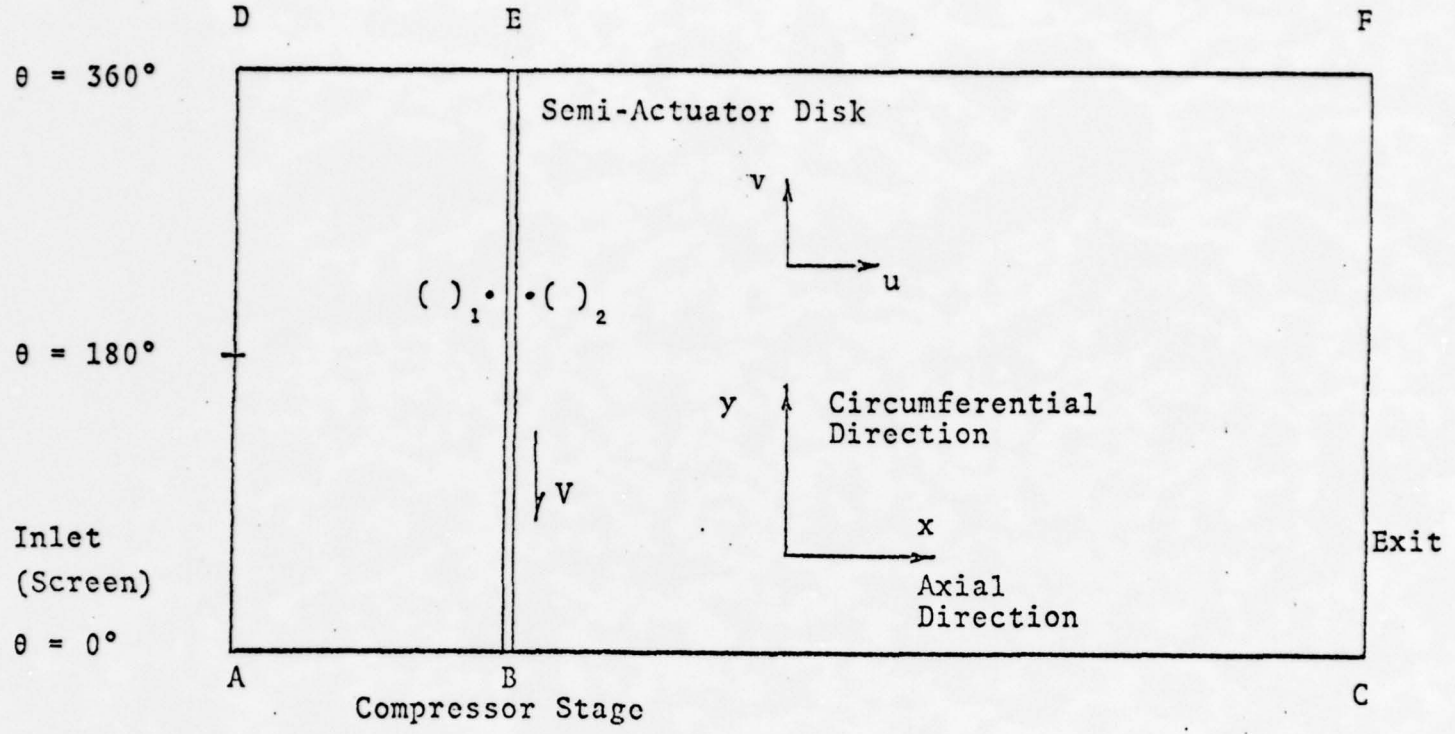

Fig. 1 Schematic Diagram of Compressor Flow Field with Semi-Actuator Disk Representation of Blade Row.

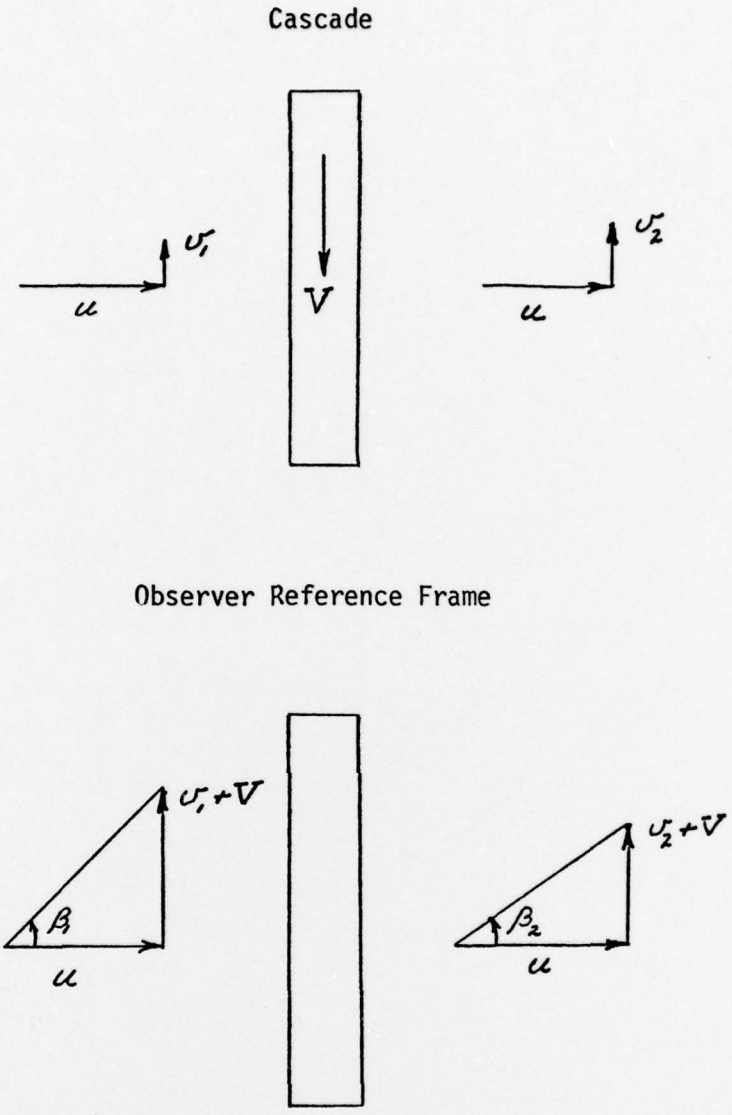

Figure 2 Velocity Diagrams in Stationary and Rotating Reference Frames.

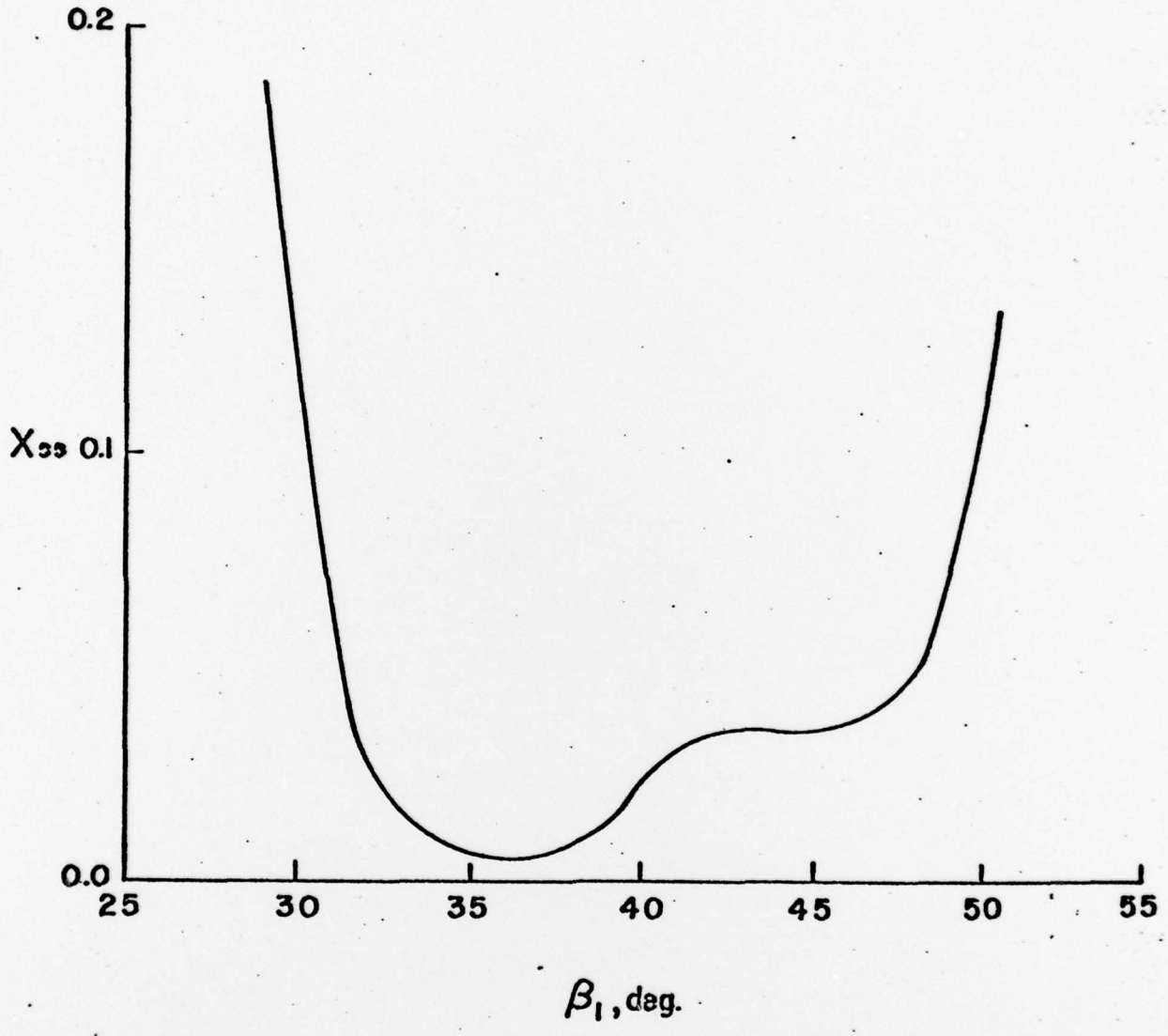

Figure 3 Steady State Loss Coefficient as a Function of Inlet Angle.

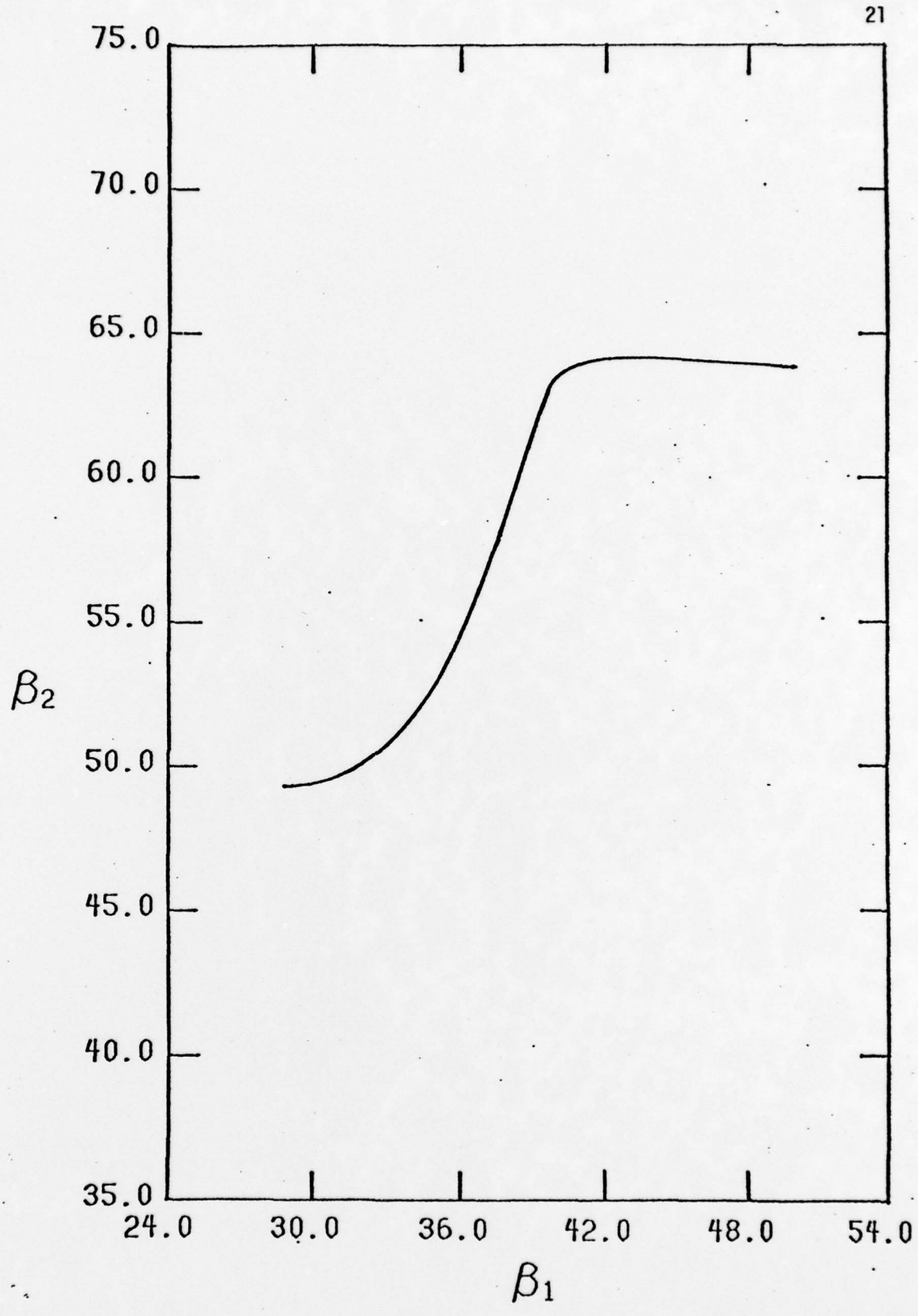

Figure 4 Turning Angle as a Function of Inlet Angle.

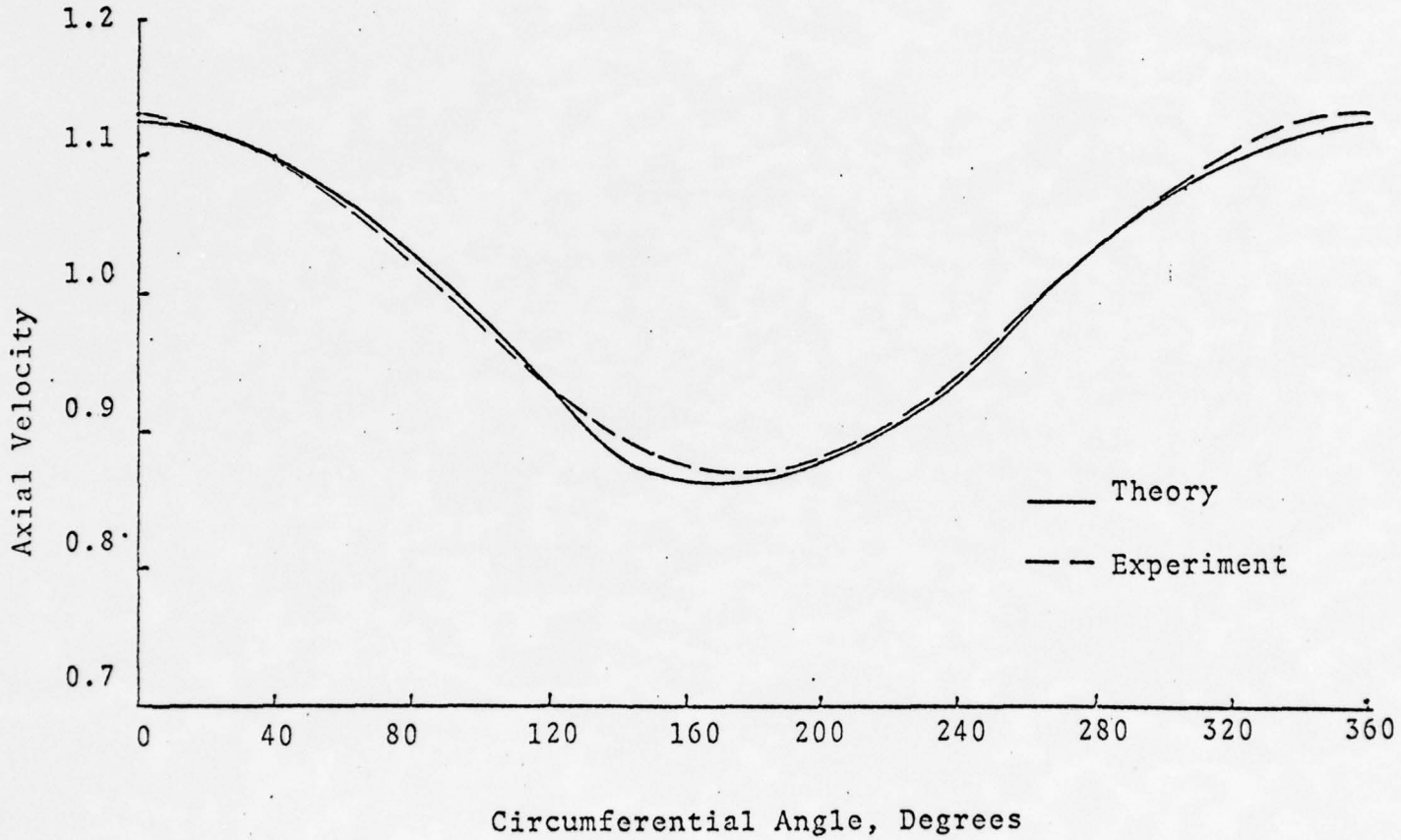

Fig. 5 Comparison of Upstream Axial Velocity Distortion Profiles.

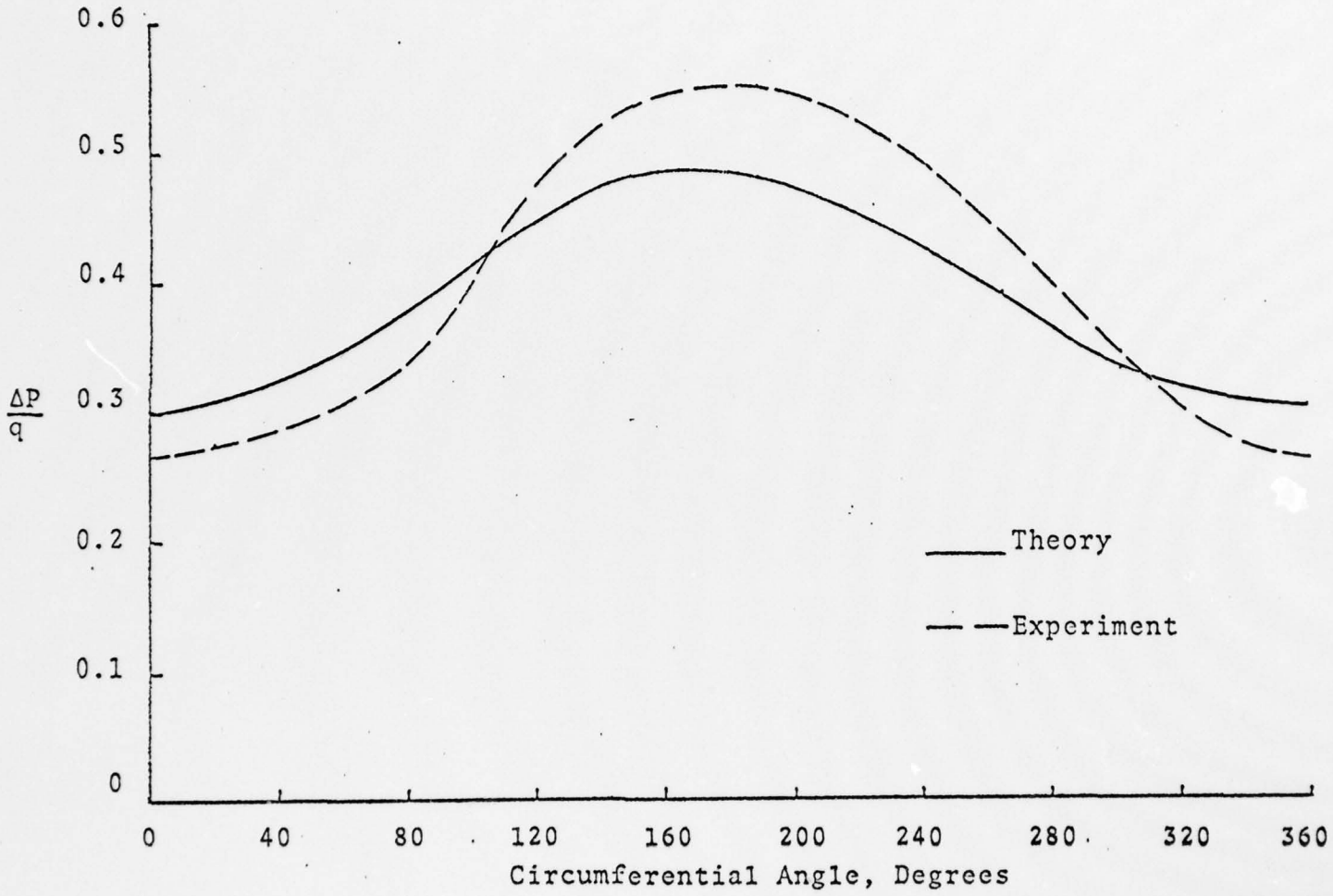

Fig.6 Comparison of Static Pressure Rise Across Blade Row.

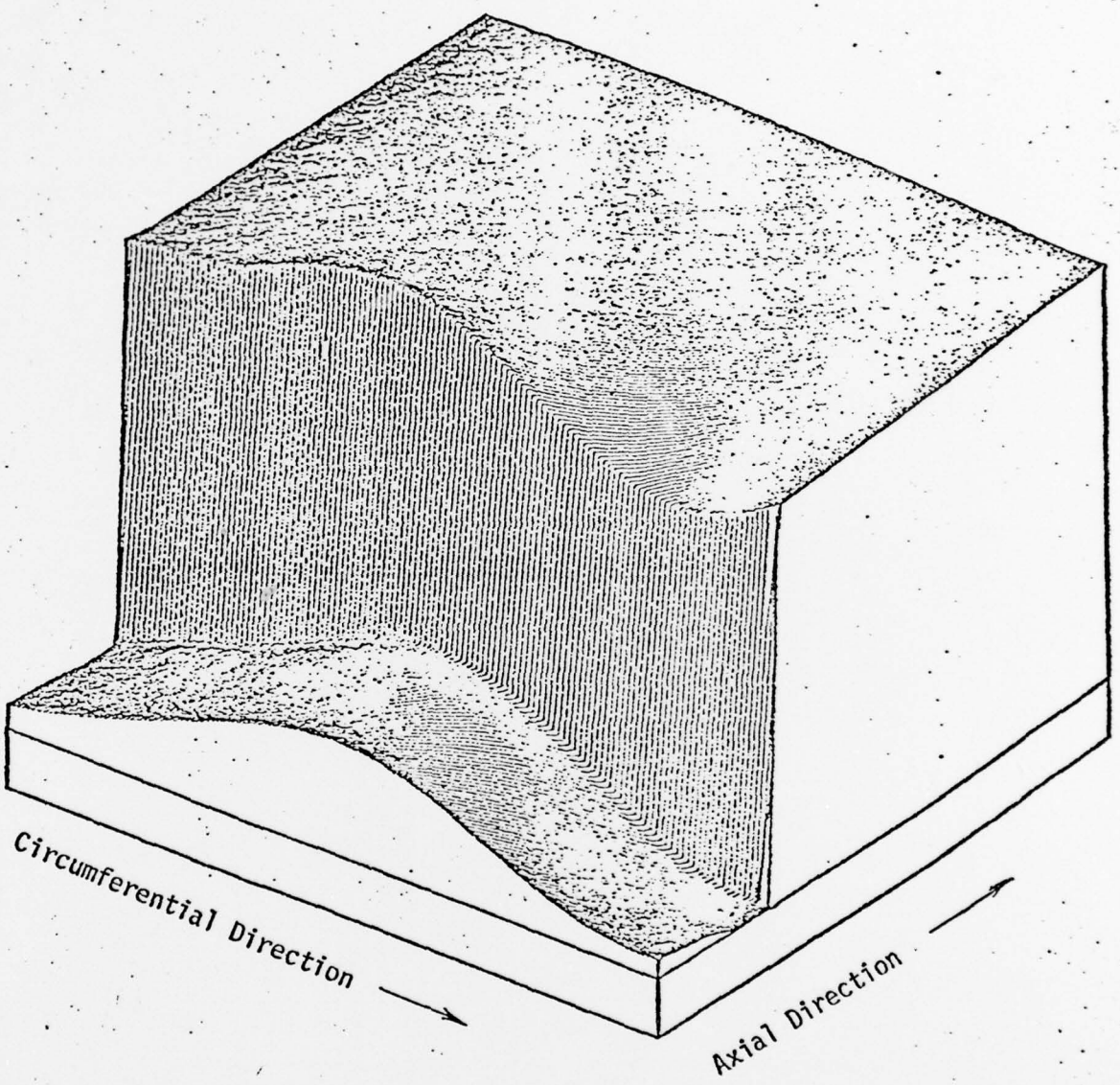

Figure 7 Static Pressure Field.

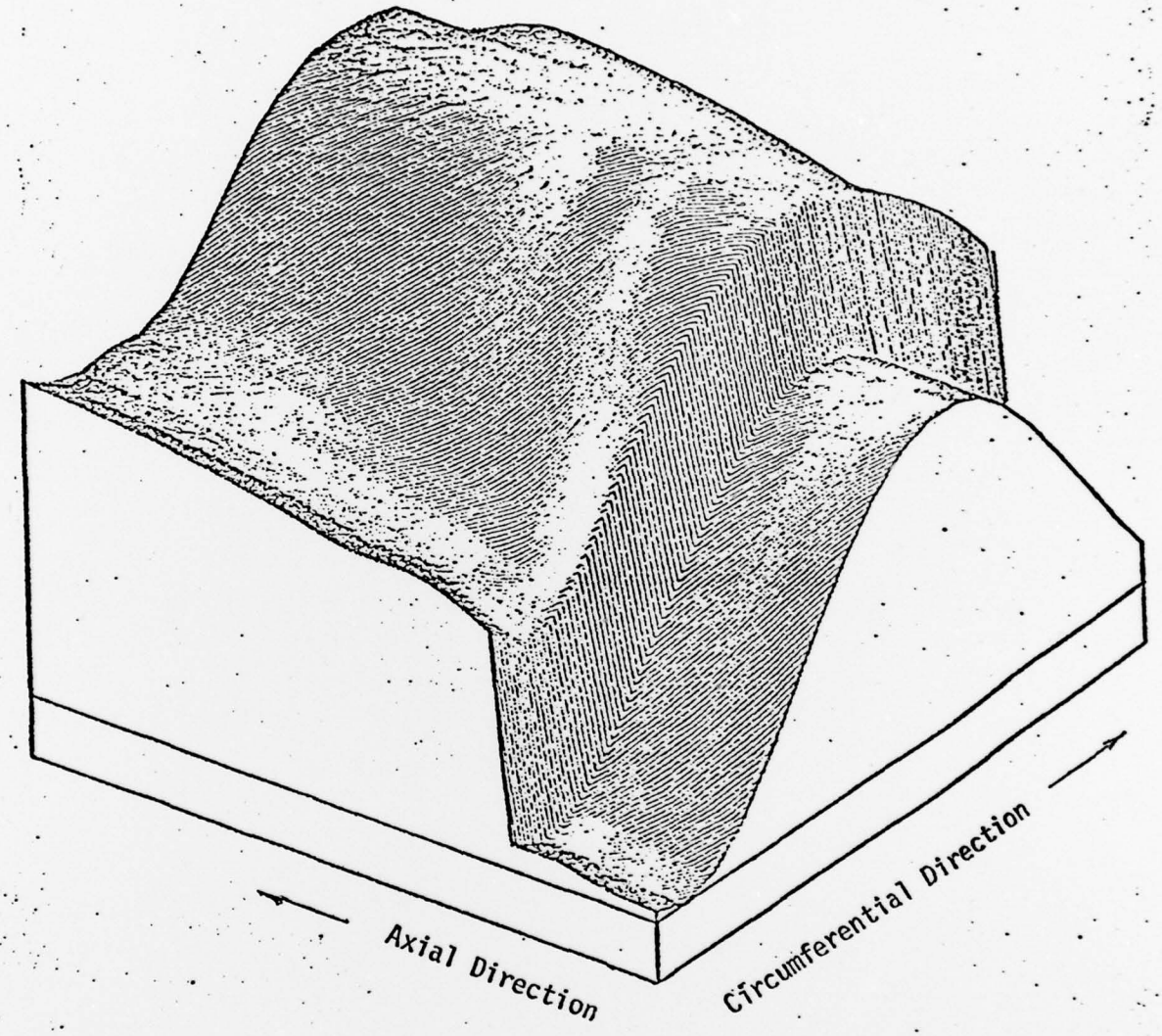

Figure 8 Total Velocity Field.

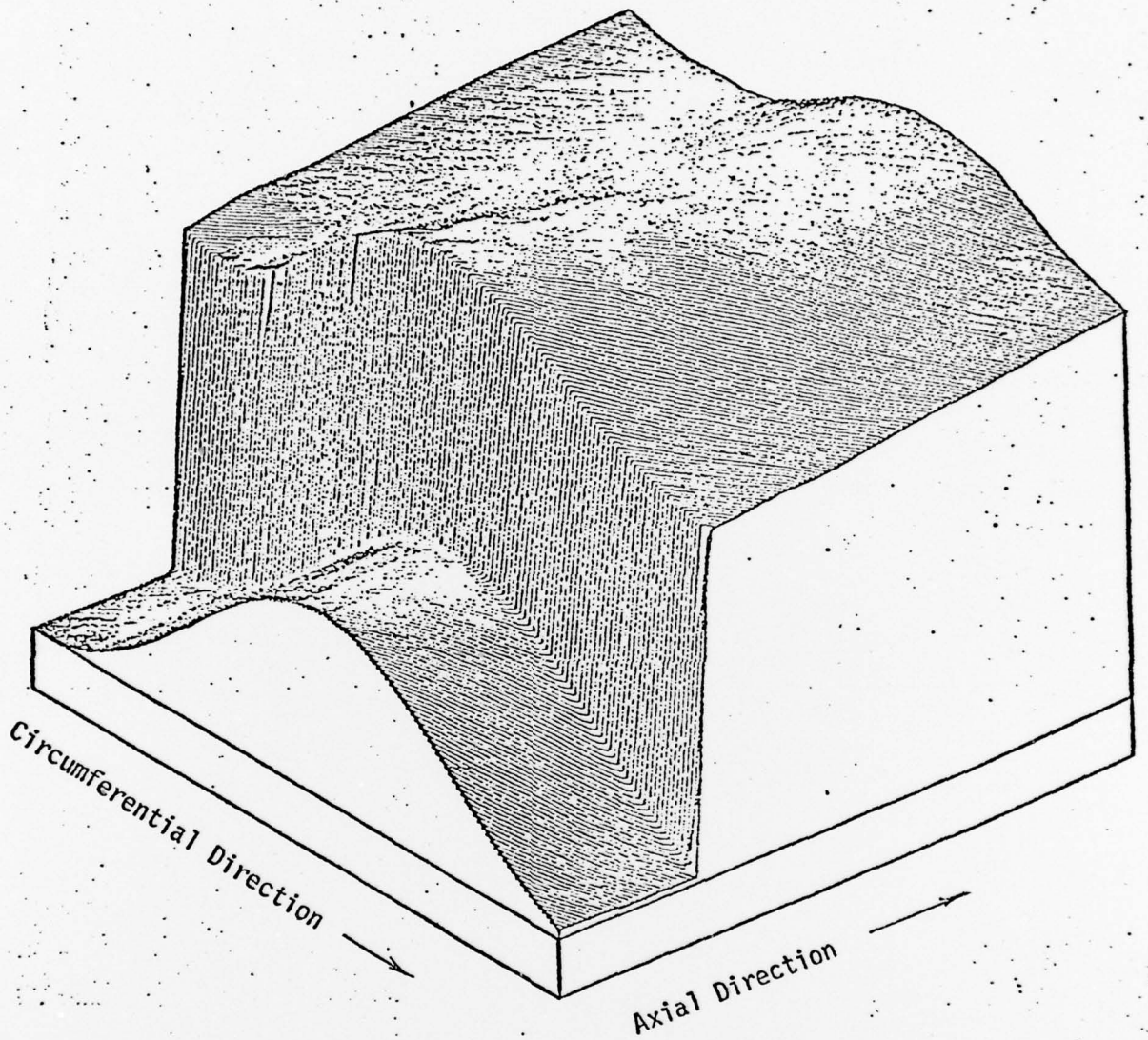

Figure 9 Total Pressure Field.

Unclassified
SECURITY CLASSIFICATION OF THIS PAGE (When Data Entered)

REPORT DOCUMENTATION PAGE		READ INSTRUCTIONS BEFORE COMPLETING FORM
1. REPORT NUMBER (14) NCSU/EDC-79-1	2. GOVT ACCESSION NO.	3. RECIPIENT'S CATALOG NUMBER
4. TITLE (and Subtitle) (6) An Actuator Disk Analysis of an Isolated Rotor with Distorted Inflow.		5. TYPE OF REPORT & PERIOD COVERED (9) Technical Report. Jan 1976 - Dec 1978
		6. PERFORMING ORG. REPORT NUMBER NCSU/EDC-79-1
7. AUTHOR(s) (10) John N. Perkins		8. CONTRACT OR GRANT NUMBER(s) (15) F44620-76-C-0055
9. PERFORMING ORGANIZATION NAME AND ADDRESS North Carolina State University School of Engineering, Engineering Design Center Raleigh, North Carolina 27650		10. PROGRAM ELEMENT, PROJECT, TASK AREA & WORK UNIT NUMBERS
11. CONTROLLING OFFICE NAME AND ADDRESS Air Force Office of Scientific Research Building 410 Bolling AFB, DC 20332	(11) 31	12. REPORT DATE March 1979
		13. NUMBER OF PAGES 28
14. MONITORING AGENCY NAME & ADDRESS (if different from Controlling Office) (12) 31p.		15. SECURITY CLASS. (of this report) Unclassified
		15a. DECLASSIFICATION/DOWNGRADING SCHEDULE

16. DISTRIBUTION STATEMENT (of this Report)

17. DISTRIBUTION STATEMENT (of the abstract entered in Block 20, if different from Report)

18. SUPPLEMENTARY NOTES

19. KEY WORDS (Continue on reverse side if necessary and identify by block number)
Dynamic stall
Distorted flow
Unsteady flow
Unsteady boundary layer
Turbocompressor

20. ABSTRACT (Continue on reverse side if necessary and identify by block number)
An analytical study of the passage of distorted flow through an isolated, high hub-tip ratio axial compressor is reported. The analysis involves the coupling of the unsteady blade row aerodynamic response (with the flow immediately upstream of the blade row prescribed) with the unsteady duct flow both upstream and downstream of the blade row under the influence of the blade row loading. The numerical solution uses a starting procedure which does not require the inlet plane to be far enough upstream to be unaffected by the presence of the blade row. Hence any experimentally determined distortion at any arbitrary

DD FORM 1 JAN 73 1473 EDITION OF 1 NOV 65 IS OBSOLETE Unclassified
SECURITY CLASSIFICATION OF THIS PAGE (When Data Entered)

409 679

distance upstream of the blade row can be modelled. The results obtained indicate that the predicted pressure profile at the blade row exit is strongly dependent on the experimentally determined steady-state loss and exit flow angle curves, but is almost independent of the magnitude of the first order lag coefficient used to represent the boundary layer time delay through the blade passages.